POSTDEADLINE PAPERS

1995

PHOTOSENSITIVITY AND QUADRATIC NONLINEARITY IN GLASS WAVEGUIDES

FUNDAMENTALS AND APPLICATIONS

SEPTEMBER 9–11, 1995
PORTLAND, OREGON

1995 TECHNICAL DIGEST SERIES
VOLUME 22

Sponsored and Managed by
Optical Society of America

DISCLAIMER NOTICE

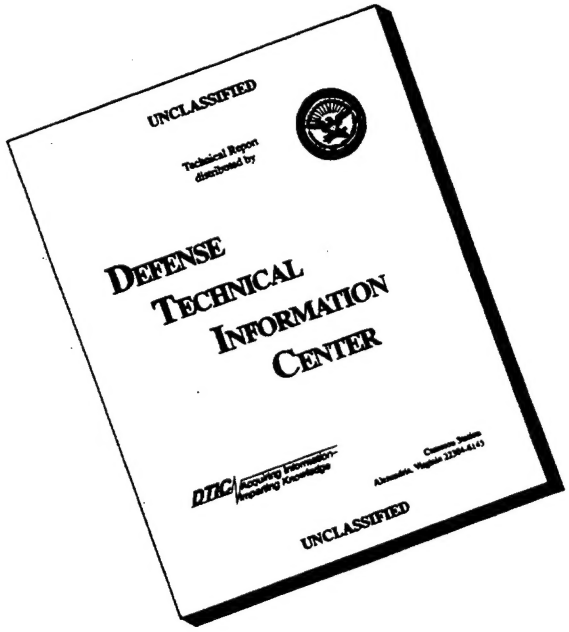

THIS DOCUMENT IS BEST QUALITY AVAILABLE. THE COPY FURNISHED TO DTIC CONTAINED A SIGNIFICANT NUMBER OF PAGES WHICH DO NOT REPRODUCE LEGIBLY.

Sunday, September 10, 1995
4:45pm - 6:00pm
Multnomah Room
Red Lion Hotel Lloyd Center
R. P. Salathe, Swiss Federal Institute of Technology, Presider

PD1 4:45pm 5:00pm — Novel technique for writing long superstructured fiber bragg gratings, Raoul Stubbe, Benet Sahlgren, Simon Sandgrew, Adel Asseh, Royal Inst. of Tech., Sweden.....

PD2 5:00pm 5:15pm — Photobleaching of broadband absorptions associated with the formation of single-pulse fiber bragg gratings, Charles G. Askins, Martin A. Putnam, E. Joe Friebele, Naval Research Lab., USA.....

PD3 5:15pm 5:30pm — Photoinduced structural transformation in silica glass: mechanism for uv-written refractive index gratings?, V. B. Sulimov, V. O. Sokolov, Eugenii M. Dianov, Bertrand Poumellec, Academy of Sci. of the USSR, Russian Federation.....

PD4 5:30pm 5:45pm — Second-harmonic measurements in uv-assisted electrically- poled glasses, Alice C. Liu, Michel Digonnet, Gordon S. Kino, Stanford Univ., USA.....

PD5 5:45pm 6:00pm — Directly UV-written erbium doped waveguides, Jorg Hubner, Thomas Feuchter, Christian V. Poulsen, Martin Kristensen, Mikroelektronik Cntr., Denmark.....

Novel technique for writing long superstructured fiber Bragg gratings

Raoul Stubbe, Bengt Sahlgren, Simon Sandgren and Adel Asseh*

Institute of Optical Research, S-100 44 Stockholm, Sweden
* Royal Institute of Technology, Physics II, S-100 44 Stockholm, Sweden

Abstract

We have developed and demonstrated a novel technique to manufacture very long and superstructured gratings based on writing a set of consecutive subgratings with interferometric control of the relative position between the subgratings.

Introduction

Beginning with the pioneering demonstration by Meltz et al. [1] a whole new class of fiber components and devices based on fiber Bragg gratings has emerged since with a wide range of applications in fiber-optic sensors and telecommunication [2]. Many of these applications require an additional superstructure to the fiber Bragg grating, for example a chirp, a DFB structure or an apodization. The versatility of some of these components is also largely dependent on the overall length of the grating structure [3], [4]. A method for writing very long gratings has been described by Martin et al [5] where a UV-beam is scanned over a long phase mask in a fixed relative position to the fiber. The superstructure can be added by varying the exposure time or by post-processing the grating changing the DC-level of the refractive index [6]. Another method is to use specially designed long phase masks where the superstructure already has been implemented in the mask itself [7].
In this paper we present an alternative method to produce very long gratings with arbitrary grating profiles. A block diagram of the principle is shown in Figure 1. The idea is similar to the point-by-point writing method demonstrated by Hill et al. [8] only here, instead of writing a grating element at a time, a subgrating, ie a number of grating elements, is written per irradiation step. The UV-footprint creating this subgrating is accomplished either by an interferometer or a phase mask. The fiber is translated with constant speed relative to the UV-fringes with an interferometer controlled translation stage. The position is very accurately tracked during the motion and this data is used to trigger the UV-laser when the fiber reaches the desired position for the next irradiation. The relatively low relative speed between the fiber and the UV-fringes, makes their relative position virtually constant during the short (10ns) exposure time defined by the UV-laser pulse.
A natural way to generate the superstructure of the grating using the described method to fabricate gratings, is to keep the grating period of each subgrating constant but varying the phase between the subsets [9]. The number of gratings elements written in each subset gives the flexibility, the shorter the subgrating the more the average period can change per unit length.

Experimental

The fiber subject to exposure is slightly stretched between two chucks on a holder. The maximum distance between the chucks is at present 140mm. The holder is mounted on a airbearing borne carriage which is translated by a feedback controlled linear drive. The carriage can be translated over 50 cm, so in principle it would be possible to write 50 cm long gratings with this set-up. A UV-footprint is accomplished by a Mach-Zender interferometer. A second interferometer utilizing a stabilized He-Ne as lightsource continuously tracks the relative position between the fiber holder and the UV Mach-Zender. A Pockels cell is used for modulation of the tracking interferometer in order to achieve fringe counting, phase interpolation and the direction of motion. The resolution in position is 0.1nm. The tracking signal is used partly to feedback the translation stage, keeping the stage at constant speed and compensating for vibrations, partly to trigger the UV-laser when the position reaches a value that has been predefined in a computer where the grating profile data have been

calculated. The fiber can be moved back and forth and thus we are able to do multiple exposures, and in principle accomplish apodisations this way.
To test the capability of the setup we wrote gratings without any superstructures, keeping the UV-exposure at a very low level. This to make sure that the reflectance would not reach 100% despite the length of the grating. We have written several 10 cm long gratings while following the growth by measuring the reflectance with a spectrum analyzer and when the fiber was well aligned with the motion, a completely continuous growth of the gratings could be observed. There were no signs in the spectrum pointing at systematic phase errors such as stitching errors. Furthermore we have measured the linewidth of the gratings using both a tunable DBR-laser and a Fourier transform spectrometer [10]. The results are similar and give linewidths about 15-20 pm, see Figure 2a,b. A numerical calculation of such a grating at 1550 nm, gave an expected linewidth of 4pm. We assume that the slightly larger linewidth can be explained by strain and temperature gradients along the grating. We also wrote a 14 cm long grating, but this grating turned out to have a linewidth that was larger than the 10 cm gratings which also indicates that we have reached a region were temperature control and strain control will be necessary. In addition, we have also made numerical simulations where we introduced random errors in the phase difference between subgratings The results show that the random errors of our gratings are smaller than 10 nm.

Furthermore we have used this setup to fabricate a 10 cm grating with a $\pi/2$ phase shift in the middle of the grating in an Yb^{3+}-doped fiber to form a fiber DFB-laser [4] and to make chirped gratings with a very linear chirp [11].

Conclusion

We have developed and demonstrated a novel technique to manufacture very long and superstructured gratings. We have written a 10cm long unchirped grating with a linewidth of 19 pm. The grating spectrum shows that the gratings are of very high quality and do not suffer from stitching errors, but the theoretical value of 4pm has not been reached. The technique is very flexible has potential to become a versatile tool for fabricating gratings for special applications such as dispersion compensation, fiber lasers and special fiber filters.

Acknowledgment

The authors wish to thank H.Storøy and W. Eriksen for valuable help with the electronics of the device.

References

[1] G. Meltz, W.W. Morey, and W.H. Glenn, "Formation of Bragg gratings in optical fibers by a transverse holographic method," Opt. Lett., 14, 823, (1989)

[2] P. St. J. Russel, J-L. Archambault and L. Reekie, "Fibre Gratings," Physics World, October, (1993)

[3] P.A. Krug, T. Stephens, G. Yoffe, F. Oullette, P. Hill, and G. Dhosi, "270km transmission at 10 Gbit/s in non-dispersion-shifted fibre using adjustably chirped 120 mm fibre Bragg grating dispersion compensator, OFC´95, postdeadline papers, PD- 27, (1995)

[4] A.Asseh, H. Storøy, J.T. Kringlebotn, W. Margulis, B. Sahlgren, S. Sandgren, R. Stubbe and G. Edwall, "10cm Yb^{3+} DFB fibre laser with permanent phase shifted grating," Electron. Lett., **31**, 969, (1995)

[5] J. Martin, F.Oullette, " Novel writing technique of long and highly reflective in-fibre gratings," Electron. Lett, **30**, 811, (1994)

[6] R. Kaschyap, P.F. McKee, R.J. Campbell and D.L. Williams, "Novel method of producing all fibre photo-induced chirped gratings," Electron. Lett., **30**, 996, (1994)

[7] K.O. Hill, F. Bilodaeu, B. Malo, T. Kitagawa, S. Thériault, D.C. Johnson, J. Albert and K. Takiguchi, "Aperiodic in-fiber Bragg gratings for optical fiber dispersion compensation," OFC´94, postdeadline papers, PD-77, (1994)

[8] B. Malo, K.O. Hill, F. Bilodaeu, D.C. Johnson and J. Albert, "Point-by-point fabrication of Micro-Bragg gratings in photosensitive fibre using single excimer pulse refractive index modification techniques," Electron. Lett., **29**, 1668, (1993)

[9] U. Eriksson, P. Blixt, and J.A. Tellefsen, Jr., "Design of fiber gratings for total dispersion compensation," Opt. Lett, **19**, 1028, (1994)

[10] M.A. Davies and A.D. Kersey ,"Fiber Fourier transform spectrometer for decoding Bragg grating sensors," in Proc. of OFS´10, 167, (1994)

[11] S.Sandgren, B. Sahlgren, A. Asseh, W. Margulis, F. Laurell, R. Stubbe, and A. Lidgard, "Characterisation of Bragg gratings in fibers with the heat-scan technique," Electron. Lett., **31**, 665, (1995)

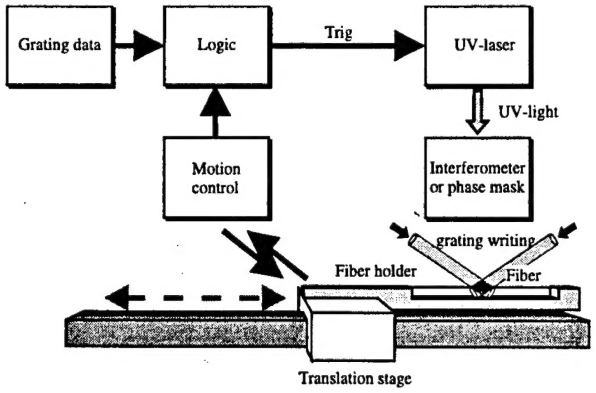

Fig. 1 Sequencial writing of fiber Bragg gratings

a)

b)

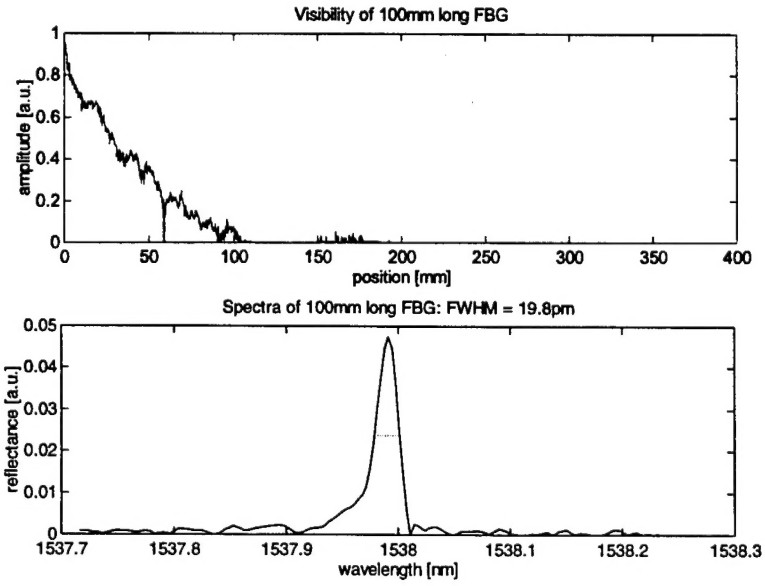

Fig 2. a) The visibility trace of the Fourier spectrometer b) The spectrum of a 10 cm FBG

Photobleaching of broadband absorptions associated with the formation of single-pulse fiber Bragg gratings

C. G. Askins, M. A. Putnam and E. J. Friebele

Naval Research Laboratory
Washington, DC 20375

Abstract: Broad spectral losses near 800 nm have been identified which arise concurrently with the formation of type 1 single-pulse fiber Bragg gratings. The losses can be reduced 7-fold with 640 nm light while minimally affecting Bragg reflectivity.

Introduction: Fiber Bragg gratings are assumed to be essentially free of absorption losses in the region of the Bragg wavelength. In at least one application area, distributed sensing, the assumption of absorptionless transmission must be closely examined. Systems are envisioned which involve precisely evaluating the Bragg wavelength of > 100 FBG's along a single fiber.[1] For reasons partly determined by detector performance, the wavelength region near 800 nm is particularly well suited for very large scale multiplexing. We have closely investigated the properties of single-pulse FBG arrays written[2] for use near 800 nm, and have discovered that a ~0.1 dB permanent loss is induced in the operational wavelength region when the FBG is written.

Experiment: Samples consisted of multiple-grating sections from stepped-wavelength arrays written on the draw tower (single pulse, type 1) in fiber drawn from an in-house preform. The fiber was a matched-clad (Ge-F-doped silica) single-mode design, with 15-20% Ge doped into the core. The fiber was drawn to have a cutoff wavelength near 730 nm; one-centimeter-diameter bend loss was minimal up to 950 nm.

Three properties of the gratings were monitored for change over the course of the experiment: optical absorption, relative reflectivity, and relative refractive index. In the part of the experiment which monitored index change, a miniature spectrometer was used to resolve wavelength shifts to within 0.001 nm. Temperature stabilization and use of reference gratings permitted sensitivity to index changes below 5×10^{-6}.

A preliminary experiment employed a 10-mW HeNe laser, but a multi-line (640 - 670 nm) Kr ion laser capable of several watts output was selected to accelerate the bleaching action. Launched power was varied during the course of the experiment so that 50 to 300 mW were detected at the output end of the fiber.

Results: Figure 1 shows optical attenuation associated with a single grating from 700 to 900 nm for the as-written case and three stages of photobleaching. Around the 810 nm Bragg wavelength, the parasitic loss is seen to bleach from the initial value of 0.07 dB to 0.01 dB. Because larger bleaching effects were evident at shorter wavelengths, the loss spectra were extended to 280 nm with short-section cutback techniques. Data at these wavelengths helped in determining whether the bleachable loss near 800 nm should be attributed to tails of deep-uv bands, or to as-yet unreported lower energy absorptions. Spectra including the

additional data are plotted as absolute absorbance (optical density per cm) vs energy (eV) in Figures 2 and 3; these data will be treated in the discussion section.

Although a 7-to-1 reduction is seen in the parasitic loss near 800 nm, the measured reflectivities of the gratings are only slightly affected. Figure 4 shows both the normalized parasitic loss (lower curve) and grating reflectivity after progressive exposure to the Kr laser fluence. Following a several hour exposure totalling > 3 kJ, the bleaching rate has greatly slowed, and over 80% of the initial reflectivity remains. By tracking the Bragg wavelengths of several gratings, we were able to demonstrate that the average index in the vicinity of the gratings changed by less than 5.0×10^{-6}.

Single-pulse FBGs are known to experience the onset of erasure above 200 C. A heat flow calculation predicts that the bleaching laser at 300 mW induces a temperature rise of less than 80 C. To examine the possibility of a thermal contribution to bleaching, an array was held at 150 C for three hours; less than a 3% change in the induced broadband absorption resulted.

Discussion: The large reduction in absorption without significant index changes argues that resonances accessible to our spectral attenuation measurements are not primarily responsible for the index modulation. Gaussian fits to the data were attempted to resolve the loss near 800 nm into components arising either from reported absorptions at and above 3.8 eV, or from other bands. The intrinsic spectrum (Fig. 2) can be fit by bands at 5.125 eV (242 nm) and 3.83 eV (390 nm)[3-5].

The center energies and widths of these two components formed the basis of a fit to the fully bleached spectrum (Fig. 3, heavy curve) where the addition of a band near 4.25 eV (292 nm) was clearly required. Such a feature has been attributed to the Ge(1) defect during the preparation of fibers for SHG[6]. Consistency with partially bleached spectra required that the loss below 3.3 eV be accounted for by at least two more bands. While the center energies and widths are not exact, Gaussians at 2.49 eV (498 nm) and 3.18 eV (390 nm) allow excellent agreement with the data below 3.0 eV. Figure 3 also shows the spectrum of the as-written grating fitted by appropriate amplitude adjustments to the 5 Gaussians.

Because these spectral data extend only to 280 nm, the projected values for amplitude, width and center energy of the 5.125 eV band are not rigorous. It is worth noting, however, that the accepted amplitudes and widths from the literature are incompatible with a simple resolution of the intrinsic spectrum with two bands. Further, the 5.125 eV band is generally bleached by multiple-pulse grating formation; here, the high energy band unambiguously *increased* with the writing exposure.

The 5.125, 4.25 and 3.83 eV bands account well for the short-wavelength portion of the spectrum, but they do not contribute appreciable loss in the vicinity of 800 nm. Previously unreported bands near 2.5 and 3.2 eV appear to dominate the bleachable induced absorption in this region.

Conclusions: An excess loss mechanism which would affect the operation of large-count FBGs sensor arrays operating near 800 nm has been identified. This loss can be reduced by at least 7:1 by photobleaching with 640 nm laser light. While removing 85% of the excess loss, the treatment leaves over 80% of the reflectivity of single-pulse FBGs intact. A small ($5 - 10 \times 10^{-6}$) average index change should accompany the bleaching process, so

this process may also be implied in stabilizing the Bragg wavelength of fiber gratings.

References

1. C.G. Askins, M.A. Putnam and E.J. Friebele, "Instrumentation for interrogating many-element fiber Bragg grating arrays," in Smart Sensing, Processing, and Instrumentation (Vol. 2444), W.B. Spillman, Jr., Ed. (SPIE, Bellingham, WA, 1995) pp. 257-266.

2. C.G. Askins, M.A. Putnam, G.M. Williams and E.J. Friebele, "Stepped-wavelength optical-fiber Bragg grating arrays fabricated in line on a draw tower," Opt. Lett. **19** (1994) 147-149.

3. J. Yuen, "Ultraviolet absorption studies of germanosilicate glasses," Appl. Opt. **21** (1982) 136-140.

4. R.M. Atkins, "Measurement of the ultraviolet absorption spectrum of optical fibers," Opt. Lett. **17** (1992) 469-471.

5. H. Hosono, Y. Abe, D.L. Kinser, R.A. Weeks, K. Muta and H. Kawazoe, "Nature and origin of the 5-eV band in SiO_2:GeO_2 glasses," Phys. Rev. B **46** (1992) 11445-11451.

6. E.J. Friebele and D.L. Griscom, "Color centers in glass optical fiber waveguides," Defects in Glasses (MRS Proceedings Volume 61), F.L. Galeener, D.L. Griscom and M.J. Weber, Ed. (Materials Research Society, Pittsburgh, PA, 1986), pp. 319-331.

7. M. Gallagher and U. Osterberg, "Spectroscopy of defects in germanium-doped silica glass," J. Appl. Phys. 74 (1993) 2771-2778.

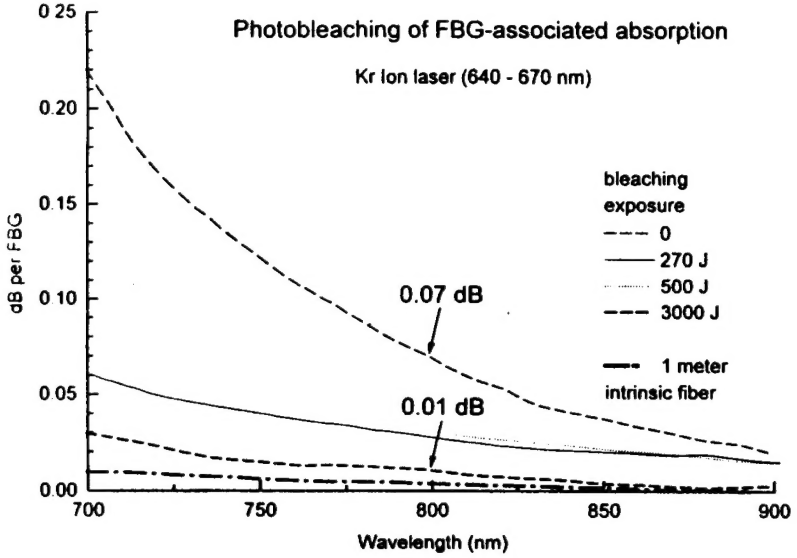

Figure 1. Optical absorption induced by FBG formation measured near 800 nm, and photobleaching with 640 nm laser light.

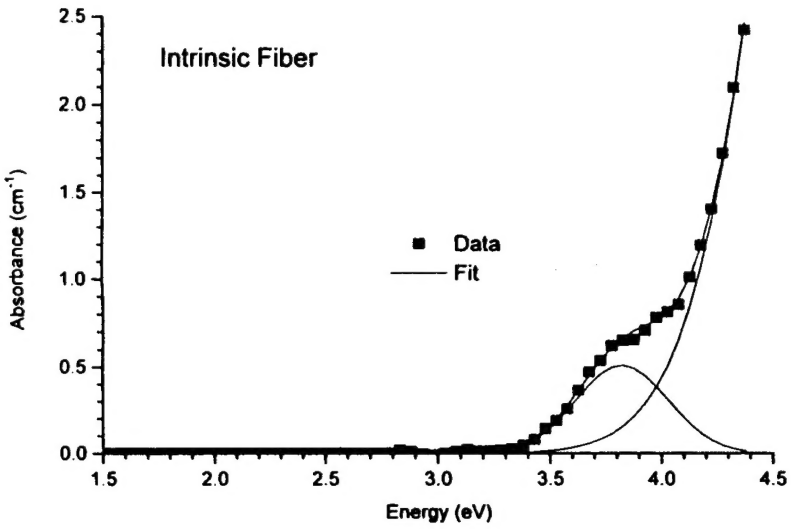

Figure 2. Intrinsic loss in fiber with no gratings. Data are fit by two Gaussians at 5.12 eV and 3.83 eV.

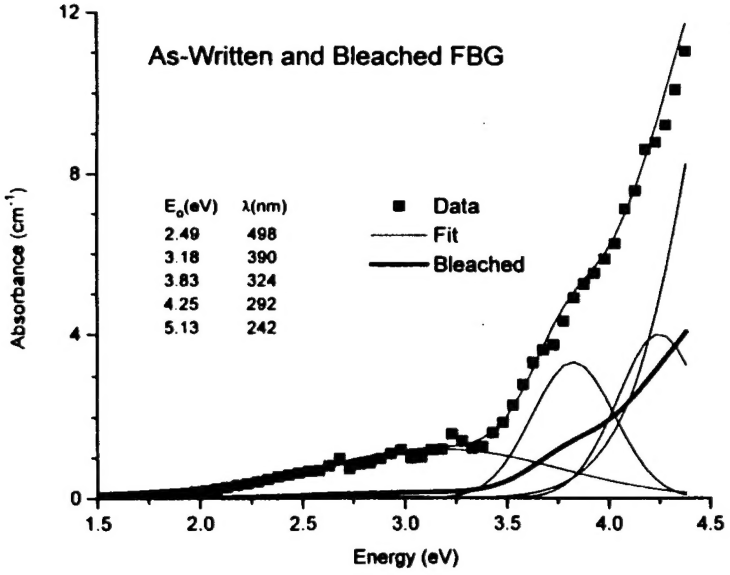

Figure 3. Optical spectra of as-written and fully bleached grating with the 5 Gaussians required to fit all data sets.

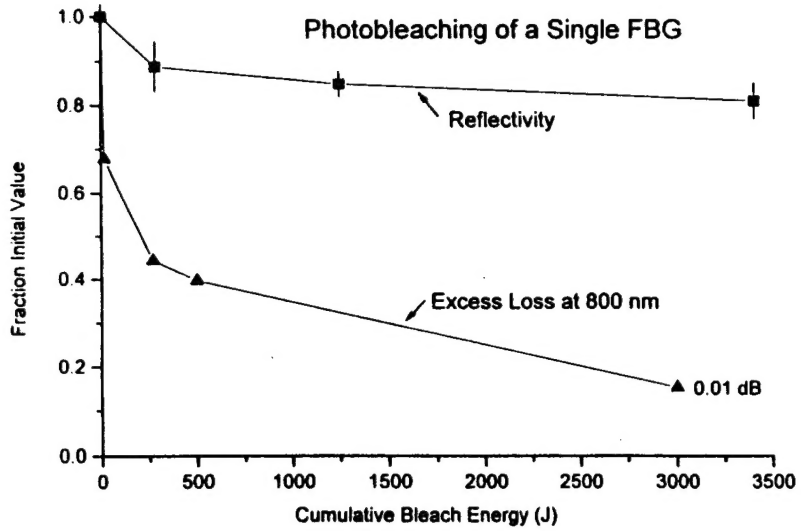

Figure 4. While absorption loss is decreased from 0.07 to 0.01 dB per grating at 800 n reflectivity is reduced by only 20%.

PHOTOINDUCED STRUCTURAL TRANSFORMATION IN SILICA GLASS: MECHANISM FOR UV-WRITTEN REFRACTIVE INDEX GRATINGS?

V.B. Sulimov, V.O. Sokolov, E.M. Dianov, B. Poumellec†

Fiber Optics Research Center at General Physics Institute, 38 Vavilov Street, Moscow 117942, Russia, Fax: (007)(095)135 81 39, tel. (007)(095)337 95 08;
†Lab.CNS, Bat. 415, URA CNRS 446, University Paris Sud, Centre d'Orsay, 91405 Orsay, France, Fax: (033)(1)69 85 54 84, tel.(033)(1)69 41 63 51

Photoinduced transition in silica glass from quartz- to rutile-like structure initiated by a strong relaxation of excited oxygen vacancies is proposed as a cause of refractive index change.

PHOTOINDUCED STRUCTURAL TRANSFORMATION IN SILICA GLASS: MECHANISM FOR UV-WRITTEN REFRACTIVE INDEX GRATINGS?

V.B. Sulimov, V.O. Sokolov, E.M. Dianov, B. Poumellec†

Fiber Optics Research Center at General Physics Institute, 38 Vavilov Street, Moscow 117942, Russia, Fax: (007)(095)135 81 39, tel. (007)(095)337 95 08;
†Lab.CNS, Bat. 415, URA CNRS 446, University Paris Sud, Centre d'Orsay, 91405 Orsay, France, Fax: (033)(1)69 85 54 84, tel.(033)(1)69 41 63 51

UV-written refractive index gratings have become a key element of many modern fibre based devices such as dispersion compensators and pulse stretchers (see, for example, [1]). Despite their practical importance and popularity, the physical nature lying behind formation of fibre gratings has not been completely understood yet. In this paper, based on our extensive computer modelling, we propose a mechanism of UV-written grating formation and give an explanation to many experimentally observed facts and effects such as low thermal stability of conventional gratings and high stability of the gratings loaded with hydrogen, the increase of glass density, bleaching of oxygen-deficient centres (ODC), and generation of GeE′ centres in the course of grating formation. From our computer calculations we can also identify emission and absorption bands of silica glass.

The modelling is based on a cluster $Si_{14}O_{15}H_{26}$ of quartz (or similar cluster of GeO_2). The aim of the modelling is to find energies of an oxygen vacancy in the ground and excited states, transition energies and electron wave functions. It was found that the most suitable method for such calculations is the quantum chemical MNDO method [2] with the configuration interaction option, which allows the atomic relaxation and electron correlations to be taken into account.

Calculated energies of the ground singlet S_0, and excited triplet T_1 and singlet S_1 states are presented in Fig. 1 as functions of the distance R between central silicon atoms Si_1 and Si_2. For $R < 3.5$ Å the silicon atoms move to one another forming the Si_1–Si_2 bond. In this, normal, configuration (Fig. 2a) calculated transition energies between S_0, S_1 and T_1 states correspond well to experimentally known oxygen-deficient centres bands [3]: the absorption at 240 nm ($S_0 \rightarrow S_1$), and visible luminescence ($T_1 \rightarrow S_0$).

We have theoretically found that the excited oxygen vacancy can exist in two different configurations: normal and so called "puckered" [4]. The excitation into the puckered state results not only in glass strains causing the refractive index change, but

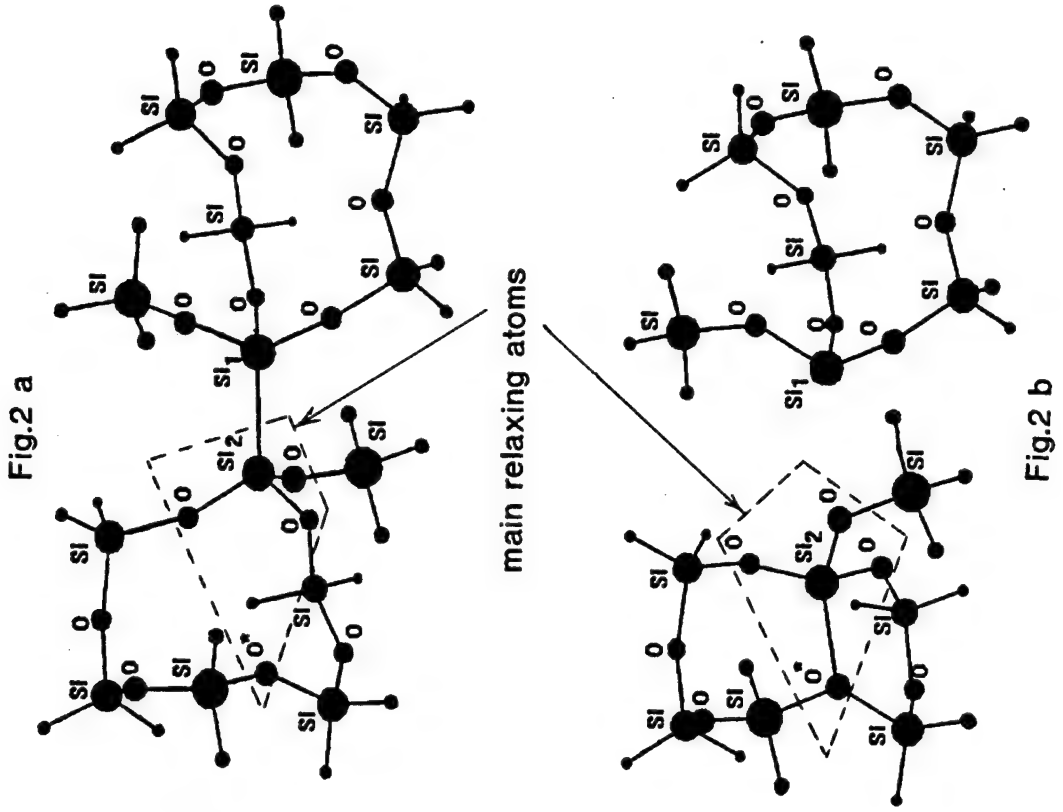

Fig.2 a

Fig.2 b

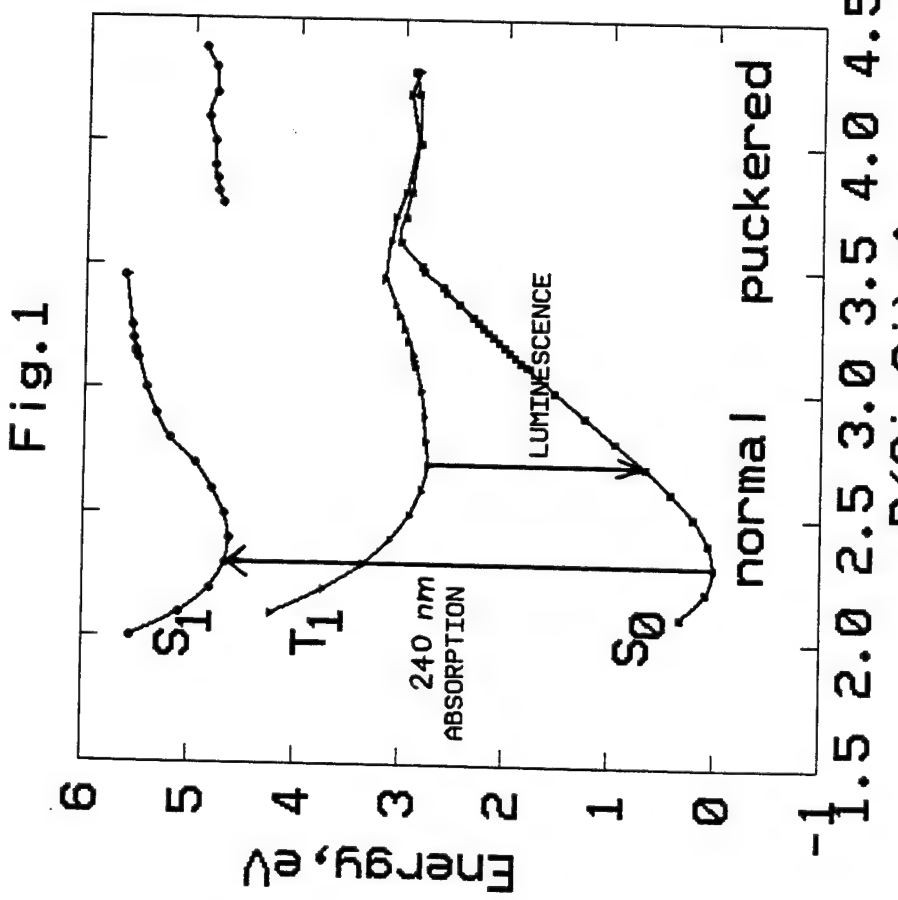

Fig.1

also makes some oxygen atoms 3-fold coordinated; their creation triggers off a phase transition from quartz-like short-range order to the more compacted rutile-like one.

Dynamics of the vacancy transition from the normal configuration to the puckered one can be described as follows. After excitation at 240 nm and following relaxation to the triplet state T_1 the vacancy can pass the energy barrier (Fig. 1) and accommodates itself in the puckered state: one of the SiO_3 pyramids adjacent to the vacancy (see Fig. 2 b) turns inside out and its silicon vertex points apart from the vacant site.

From our computer modelling we find out that:

- an absorption band of the puckered vacancy is situated far from the 240 nm band of the normal vacancy, i.e. far from experimentally observed ODC absorption band, and consequently the excitation to the puckered state bleaches 240 nm absorption band;

- there is also no ODC luminescence in the puckered state, because the energies of T_1 and S_0 states are the same (see Fig. 1);

- all observed ODC optical features, absorption band at 240 nm and visible luminescence, could be bleached by UV-excitation and relaxation of the excited vacancy from the normal to the puckered state. It explains experimentally observed ODC depletion during formation of UV-written refractive index gratings.

The generation of well known paramagnetic E′-centres was experimentally observed during the gratings formation. This can be explained in the frame of the vacancy excitation from the normal to the puckered state: if normal vacancy has no unpaired electrons and is diamagnetic then excited into the puckered state it becomes paramagnetic: one unpaired electron appears at unrelaxed 3-fold coordinated silicon atom Si_1 forming E′-centre and another one turns up at Si_2 and O^* atoms(see Fig. 2b).

The computer modelling indicates (see also [4]) that stability of the puckered vacancy is defined by the bond between the relaxed silicon atom Si_2 and an oxygen atom O^* (Fig. 2). This oxygen becomes three-fold coordinated. Such three-fold coordinated atoms are the main feature of SiO_2 rutile-type crystal (stishovite). The density of this crystal is much higher than density of quartz or silica glass. Stishovite is stable only at very high pressures and temperatures. On the contrary, germanium dioxide is stable in rutile structure under normal conditions. So, some regions in germanium doped silica glass can change their structure under UV irradiation from quartz-like type to rutile-like type. These regions must be germanium enriched. The seeds of the new phase can be the puckered oxygen vacancies containing 3-fold coordinated oxygen atoms.

Vacancies excitation in puckered state produces refractive index change by two ways. First, the strong atomic relaxation produces strains around each puckered vacancy, and these strains change the refractive index due to photoelastic phenomena. Second, the transformation of the short-range order to the rutile type increases density of glass and its refractive index. Both processes are mutually correlated: strains initiate phase transition and the latter produces strains. The estimated refractive index change due to photoelastic mechanism is about 10^{-5} for the number of puckered vacancies about 10^{18} cm^{-3}.

Experimentally observed thermal stability of the refractive index gratings can be attributed to a small energy barrier (see Fig. 1): some of the puckered vacancies could be thermally excited and relax back over the energy barrier. A stabilization of the puckered vacancy can be done by supplying the interstitial space with an element which can be bonded to relaxed silicon. For this purpose a hydrogen molecule is almost ideal: it is small enough to exist in the interstitial space, at room temperature it does not interact with saturated bonds of the perfect glass, and hydrogen molecules interact with dangling bonds in silica glass.

Thus in the hydrogen loaded silica glass the vacancy can be stabilized in puckered state by saturation of the relaxed silicon dangling bond with hydrogen atom. The formation of Si–H bond prevents the relaxation of the silicon atom back to the normal position due to the bonded hydrogen atom playing the role of an anchor.

In summary we have proposed a simple mechanism for the formation of refractive index gratings based on excitation of oxygen vacancy into the puckered state which results in refractive index change through photoelastic phenomena and transformation of the glass short-range order to more compacted one. In the frame of this picture many experimentally observed phenomena can be explained and some new effects can be predicted which will be reported at the conference.

REFERENCES

1. R.Kashyap, Optical Fiber Technology, **1**, 17 (1994).
2. J.J.P.Stewart, *MOPAC Manual* (6th ed.), F.J.Seiler Res. Lab., U.S.A.F. Acad., *QCPE* # 455; *QCMP* # 113 (1990).
3. V.B.Sulimov and V.O.Sokolov, J. Non-Cryst. Solids (1995) (to be published).
4. K.C.Snyder and W.B.Fowler, Phys.Rev. B **48**, 13238 (1993).

Second-harmonic measurements in UV-assisted electrically-poled glasses

A. C. Liu, M. J. F. Digonnet, and G. S. Kino
Edward L. Ginzton Laboratory,
Stanford University, Stanford, CA 94305

Abstract: We report measurements of the nonlinearity induced in different glasses by UV-assisted electrical poling. Nonlinearities are found to be at best comparable to that of thermally-poled silica.

Summary: The prospect of new electro-optic silica fiber devices fabricated by electrical poling has recently stimulated considerable interest.[1-6] The original process, thermal poling,[1] produces a nonlinear region 1-3 μm thick with a nonlinear coefficient d_{33} in the range of 0.15-1 pm/V.[1-5] A possible mechanism is that poling produces either space charges or oriented dipoles, which create a strong internal electric field, which in turn induces a $\chi^{(2)}$ by rectification of the third-order susceptibility of silica.[2] Although respectable, this d_{33} value is still insufficient to produce short, low-voltage guided-wave electro-optic devices. More recently, a much larger nonlinearity was observed by room-temperature poling a Ge-doped fiber exposed to both 193-nm radiation (36 mJ/cm^2, 10 Hz) and an ≈80 V/μm field for ≈ 10 min.[6] Phase modulation measurements suggested a d_{33}≈6.6 pm/V[6] prevailing across the core (estimated at 5 μm).

The objective of this work was to attempt reproducing these figures by applying UV-assisted poling to bulk glass samples. Four types of glasses were tested: (1) Infrasil 302, (2) Herasil 1, (3) a multicomponent germanate glass containing no silica, and (4) the core of a multimode silica fiber preform with 19 mole % GeO_2. The samples were typically 0.5-1.6 mm thick and 4-25 mm across. Poling was done by placing a sample between machined Al electrodes with small transverse dimensions (to avoid air breakdown). The focused UV beam from a pulsed ArF excimer laser (193 nm, 10 Hz) was delivered to the sample through a nominally 200-μm diameter aperture drilled in the middle of the cathode. In all measurements, the UV pulse energy launched in the sample was 0.23 mJ, and the energy density per pulse at the anode in the range of 0.73-1.18 J/cm^2. After poling, the samples were characterized by second harmonic generation (SHG) measurements using the set-up shown in Fig. 1, described in greater detail elsewhere.[2] Pulses from a Q-switched 1.064-μm Nd:YAG laser were focused onto the sample at an angle θ from normal incidence. The 532-nm second harmonic (SH) power generated in the sample was measured with a calibrated photomultiplier tube (PMT). The SHG conversion efficiency η is defined as the ratio of the SH power to the square of the 1.064-μm power

launched into the sample. As shown elsewhere,[2] η was found to increase from zero at normal incidence (due to the poled region symmetry) to a maximum value for angles θ just below some angle θ_{TIR}. Above θ_{TIR}, total internal reflection of the SH signal occurs on the back surface of the sample and no SH signal is observed. In the following we only report the maximum value of η. For non-phase-matched SHG, assuming a constant d_{33} over a region of thickness l, η is proportional to the square of $d_{33}l$,[2] an important quantity in switch design.

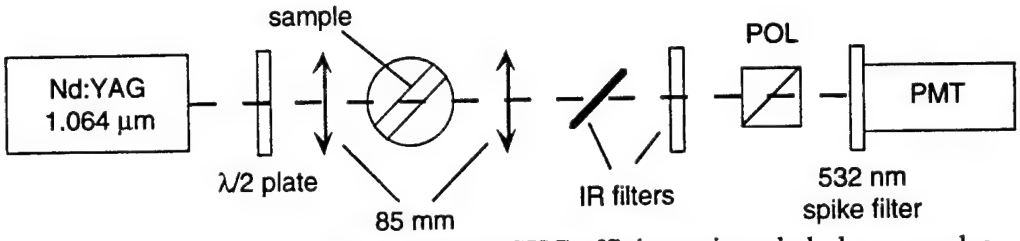

Fig. 1. Experimental setup used to measure SHG efficiency in poled glass samples.

Comparison between measurements on Infrasil samples of different thicknesses poled for 35 min at various voltages showed that η depends on the sample thickness (as well as voltage), unlike suggested by other reports for thermal poling.[1] In fact, η grows linearly with the poling field (see Fig. 2). This is true up to the maximum poling field we could apply ($\approx$ 40 V/μm) before the onset of breakdown in air around the sample.

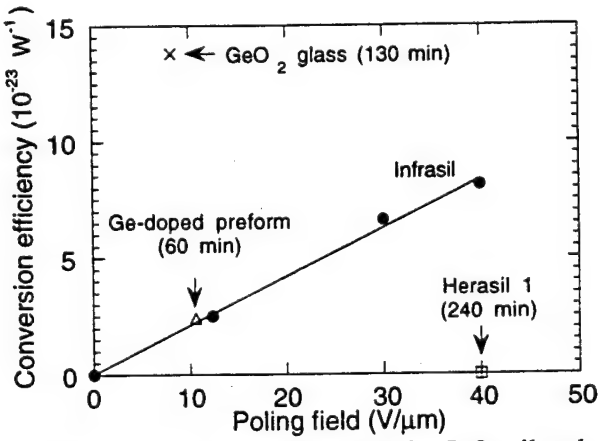

Fig. 2. Conversion efficiency vs poling field for Infrasil poled for 35 min, and highest efficiency observed in the other three glasses poled for the duration shown.

To demonstrate higher conversion efficiency, we repeated poling at 40 V/μm with increasing exposure times. The efficiency grew linearly up to 2-3 hours, then sublinearly until it essentially reached a maximum value of 4.6 10^{-22} W^{-1} after $\approx$10 hours, or a total

incident energy density of 340 kJ/cm^2. When thermally poled, the same glass samples yielded a conversion efficiency (in the vicinity of the same angle θ) of $\approx 1.8\ 10^{-21}$ W^{-1}.

The highest conversion observed for the other glasses is also shown in Fig. 2. Herasil 1 gave no measurable SH signal after poling 240 min. The germanate glass had a much lower breakdown field than Infrasil and could be poled at most at 8.2 V/μm. This data point suggests that it produces a larger slope η/E. This encouraging result lends support to the hypothesis that Ge defects precursors play a role in the generation of the permanent internal E-field, as speculated elsewhere for thermal poling.[5] However, the core region of the Ge-doped preform gave surprisingly low results, comparable to Infrasil. Because of internal stresses, however, this glass had a lower optical quality after polishing, which may be partly responsible for this result.

These investigations lead to several interesting conclusions. First, the conversion efficiency measured in UV-poled silica scales like the poling field. Second, the induced nonlinearity depends strongly on the glass composition, as in thermal poling.[1,5] Third, in Infrasil the nonlinearity reaches its maximum for UV dosages around 340 kJ/cm^2, or about 2000 times higher than needed for a Ge-doped fiber.[6] Fourth, the fact that one would expect GeO_2 to help induce stronger and/or larger nonlinear regions is only partially supported by our experimental observations. More measurements are needed to identify a trend. Finally, and more importantly, if we assume that η also scales like poling field for the germanate glass (which has the highest η/E slope), Fig. 2 suggests that even at 80 V/μm we would only get $\eta \approx 1.35\ 10^{-21}$ W^{-1}, i.e. a $d_{33}l$ product around 0.25 pm/V.μm. This is comparable to values for thermal poling, but more than 100 times lower than the $d_{33}l$ product inferred for the UV-poled fiber modulator of Ref. 6 ($\approx$ 6.6pm/Vx5μm). This last result raises questions about the equivalence of the two types of devices, and/or about possible differences between the nature of the physical processes involved in each of them.

The authors are thankful to Jay Simpson at AT&T Bell Laboratories for kindly providing the Ge-doped preform.

1. R. A. Myers, N. Mukerjhee, and S. R. J. Brueck, "Large Second-Order Nonlinearity in Poled Fused Silica," Opt. Lett. 16, No. 22, 1732-1734, Nov. 1991.
2. A. C. Liu *et al*, "Characterization of the Second-Order Nonlinearity in Poled Fused Silica," in *Doped Fiber Devices and Systems*, Proc. SPIE 2289, 194-206, 1994.
3. A. C. Liu, M. J. F. Digonnet, and G. S. Kino, "Electro-optic Phase Modulation in a Silica Channel Waveguide," Opt. Lett. 19, No. 7, 466-468, Apr. 1994.
4. A. Okada, K. Ishii, K. Mito, and K. Sasaki, "Second-Order Optical Nonlinearity in Corona-Poled Glass Films," J. Appl. Phys. 74, No. 1, 531-535, July 1993.
5. L. J. Henry *et al*, "Effect of Water on the Generation of Second Harmonic in Poled Fused Silica," in *Doped Fiber Devices and Systems*, Proc. SPIE 2289, 177-184, 1994.
6. T. Fujiwara *et al*, "Electro-Optic Effect Induced by UV-Excited Poling in a Silica Fibre," 19th Australian Conference on Optical Fibre Technology, Paper PDP-3, 1994.

Directly UV-written Erbium Doped Waveguides

Jörg Hübner,
Thomas Feuchter,
Christian V. Poulsen
Martin Kristensen

Mikroelektronik Centret
Technical University of Denmark,
Bldg. 345 E, DK-2800 Lyngby,
Denmark

Phone: +45 45 25 57 60,
Fax: +45 45 88 77 62
e-mail: johu@mic.dtu.dk

Abstract

We have produced UV-written, erbium-doped glass waveguides. A planar, three-layer structure (buffer/erbium-doped core/cladding) is exposed to 193 nm excimer laser light through an aluminum mask.

Directly UV-written Erbium Doped Waveguides

Jörg Hübner, Thomas Feuchter, Christian V. Poulsen
and Martin Kristensen

Mikroelektronik Centret
Technical University of Denmark, Bldg. 345 E, DK-2800 Lyngby, Denmark
Phone: +45 45 25 57 60, Fax: +45 45 88 77 62
e-mail: johu@mic.dtu.dk

Abstract: We have produced UV-written, erbium-doped glass waveguides. A planar, three-layer structure (buffer/erbium-doped core/cladding) is exposed to 193 nm excimer laser light through an aluminum mask.

Introduction: Photoinduced refractive index structures in germanosilicate glasses have become a topic of interest since the late 1980s when Meltz et al. [1] demonstrated side-written Bragg gratings in germanium-doped optical fibers. Lately, research has extended from fibers to planar structures such as waveguides [2], and splitters and couplers [3]. UV writing of the waveguide core may provide an excellent technique for rapid prototyping and small-quantity production of planar waveguides. A similar trend can be observed in erbium-doped optical amplifiers. While the first practical optical amplifiers were demonstrated in the mid 1980s using erbium-doped optical fibers, research is now underway to demonstrate lossless integrated-optical components using thin films of erbium-doped glasses. In this paper, we report UV-writing of erbium-doped planar optical waveguides. While properties such as propagation loss and quantum efficiency are non-ideal, we have made an important first step in realizing UV-written active integrated optical components.

Experimental: We produce the two-dimensional thin-film waveguide using plasma-enhanced chemical vapor deposition (PECVD). Three layers consisting of a buffer, waveguide core, and a top cladding are deposited onto a silicon wafer. The layer thicknesses are 12 µm, 2.5 µm, and 12 µm. These dimensions are chosen to ensure single-mode operation and to prevent interaction of the optical mode with the silicon substrate. We then deposit an 0.8 µm thick layer of aluminum on top of the cladding. This layer is patterned using conventional photolithography and etching to form a mask for subsequent UV exposure.

193 nm light from an ArF eximer laser forms the waveguide. The pulse energy is approximately 200 mJ with a pulse duration of 20 ns. The beam dimensions are approximately 20 x 8 mm^2. An anamorphic Gallilei beam compressor reduces the beam to 3 mm vertically. This spot is then scanned along the axis of the 6 µm wide aluminium apperture for 25 mm to form the waveguide. The UV-induced refractive index change is estimated to be 2 x 10^{-3}. No hydrogen loading is used. Exposure to the UV light gradually ablated the aluminum film. After 5000 pulses, the film was completely removed. A sample that was exposed to an additional 15,000 pulses without the aluminum mask still produced a waveguide. We believe that this is caused by an amplification process described by Dyer et al. [4]. Further, we believe that this and the relatively high propagation losses indicate that type-II refractive index changes are responsible for the waveguide formation.

Results and discussion: Intensity profiles of the waveguides were measured by near-field imaging using a 40X microscope objective and an infrared vidicon. The optical mode is excited by butt coupling an optical fiber to the input facet of the waveguide. The waveguide supports a single mode at both 980 nm and 1550 nm.

Insertion loss and absorption spectra were measured by coupling light from a chopped, tungsten-halogen lamp into a wavelength division multiplexer. The combiner fiber was carefully aligned to the input of the waveguide and a similar fiber was used collect the light at the end of the waveguide. Transmitted light was filtered with a spectrometer, and synchronously detected with an InGaAs detector. The characterization setup is shown in figure 1.

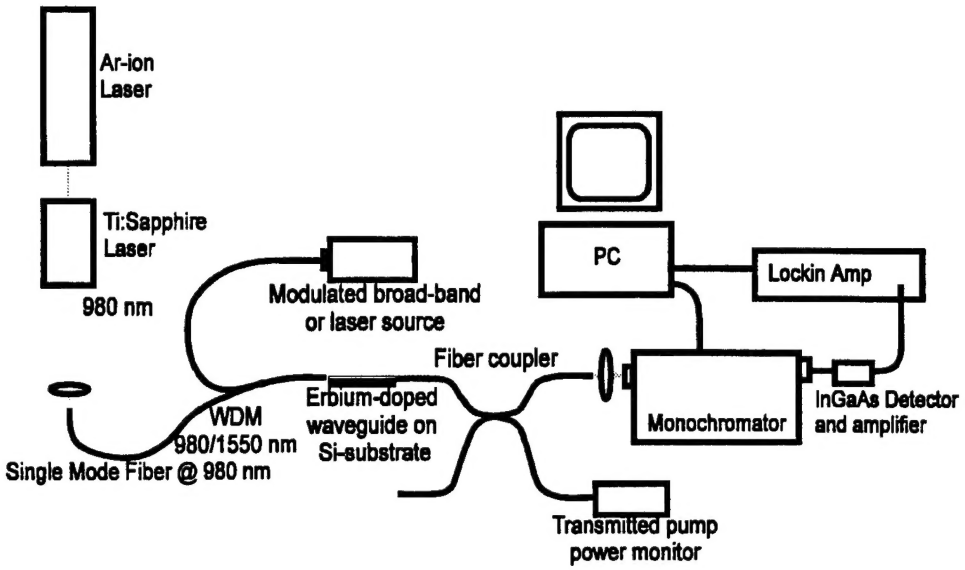

Fig. 1 Waveguide characterization setup.

A reference spectrum was recorded by coupling the white light from the excitation fiber directly into the output fiber. The absorption spectrum of the erbium-doped waveguide was normalized to this reference spectrum. Figure 2 shows the absorption spectrum recorded from a 2.5 cm long waveguide. The data indicate a background insertion loss of 6.5 dB in the erbium-free regions from 1400 nm to 1425 nm, and from 1600 nm to 1650 nm. Absorption into the $^4I_{13/2}$ level appears as a broad feature extending from 1425 nm to 1575 nm. The peak absorption of 10.5 dB at 1535 nm indicates an erbium concentration of approximately 2 wt%.

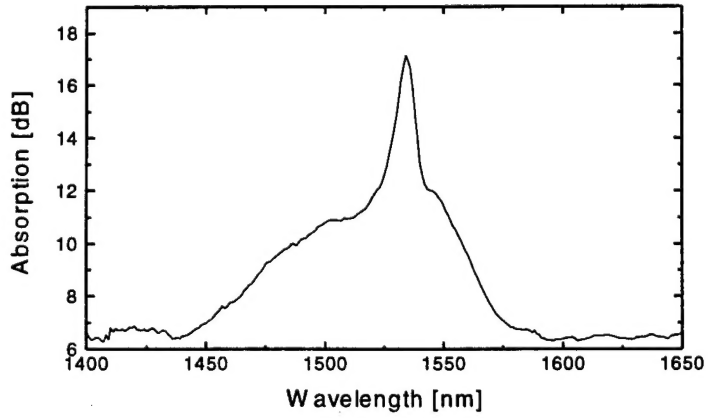

Fig. 2 Absorption spectrum of the UV-written waveguide.

By using a 980 nm / 1550 nm wavelength division multiplexer (WDM) it was possible to pump the waveguide with 180mW of 980 nm while using the white light source as signal. A large fraction of this pump light was coupled into the waveguide, thereby exciting the erbium ions situated in the core region. The transmitted white light was measured using synchronous detection thus rejecting the amplified spontaneous emission (ASE) contribution. The pump-induced change in the transmission spectrum is shown in Figure 3 and indicates a maximum of 0.8 dB for 180 mW of 980 nm pump light. The power of the white light signal was lower than the amplified spontaneous emission at the end of the pumped waveguide.

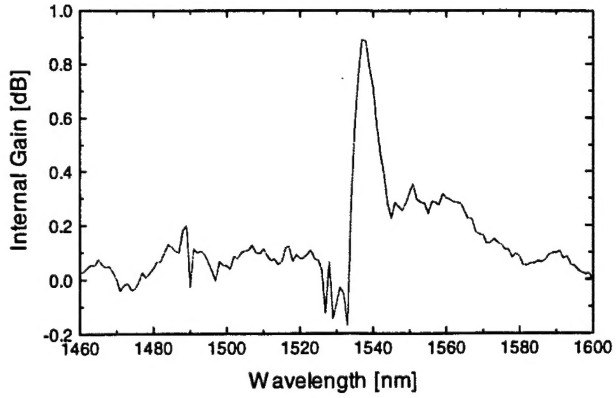

Fig. 3 Pump induced change in the absorption spectrum

The lifetime of the metastable $^4I_{13/2}$ level was measured by mechanically chopping the pump light at 8 Hz and observing the decay of the spontaneous emission using a digitizing oscilloscope after the detector. Data were recorded for the UV-exposed regions as well as unexposed regions. The decay curves shown in Figure 4 indicate a 1/e lifetime of less than 1 ms. Exposure to UV light further reduces the lifetime. This may be caused by the formation of type-II defects in the glass matrix.

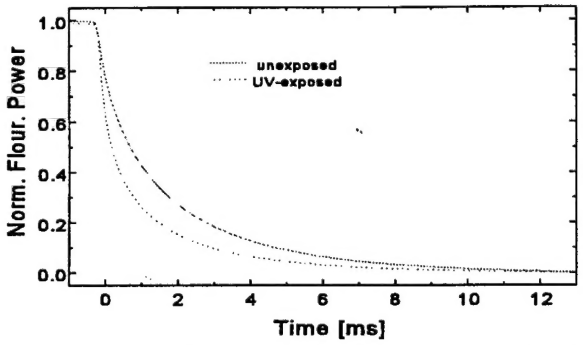

Fig. 4 Decay of the metastable $^4I_{13/2}$ erbium level at UV-exposed and unexposed regions

Saturation behavior was investigated by measuring the ASE at the end of the waveguide while attenuating the pump power. The results indicate that significantly more pump power is required to fully invert the erbium in this particular sample to achieve maximum optical gain.

Conclusions: We have produced single-mode optical waveguides in an erbium-doped thin-film glass structure using direct exposure to UV light. We believe this is the first demonstration of direct UV writing of an optical waveguide in an active glass. Preliminary results show a reduction of absorption of 0.8 dB at 1535 nm when pumped with 180 mW of 980 nm light. The measured erbium lifetime is quite short but is not unexpected since ion-ion effects are expected at such a high erbium concentration. Exposure to UV light appears to further reduce the upper-state lifetime. We expect significant improvements in erbium lifetime and optical gain with optimization of the PECVD process and UV writing procedure.

References:

[1] G. Meltz, W.W. Morey, W.H. Glenn, Opt. Lett., Vol. 14, p. 823, (1989).
[2] M. Svalgaard, C.V. Poulsen, A. Bjarklev, O. Poulsen, Electron Lett., Vol. 30, p. 1401 (1994)
[3] G.D. Maxwell, B.J. Ainslie, Electron. Lett., Vol. 31, p. 95, (1995).
[4] P.E. Dyer, R.J. Farley, R. Giedl, K.C. Byron, Electron Lett. Vol. 30, p. 1133 (1995).